ORIGINAL PAPER

Diagnosis of Diabetic Retinopathy: Automatic Extraction of Optic Disc and Exudates from Retinal Images using Marker-controlled Watershed Transformation

Ahmed Wasif Reza · C. Eswaran · Kaharudin Dimyati

Abstract Due to increasing number of diabetic retinopathy cases, ophthalmologists are experiencing serious problem to automatically extract the features from the retinal images. Optic disc (OD), exudates, and cotton wool spots are the main features of fundus images which are used for diagnosing eye diseases, such as diabetic retinopathy and glaucoma. In this paper, a new algorithm for the extraction of these bright objects from fundus images based on marker-controlled watershed segmentation is presented. The proposed algorithm makes use of average filtering and contrast adjustment as preprocessing steps. The concept of the markers is used to modify the gradient before the watershed transformation is applied. The performance of the proposed algorithm is evaluated using the test images of STARE and DRIVE databases. It is shown that the proposed method can yield an average sensitivity value of about 95%, which is comparable to those obtained by the known methods.

Keywords Diabetic retinopathy · Exudates · Cotton wool spots · Biomedical imaging and image processing · Optic disc · Watershed transformation

A. W. Reza (✉) · K. Dimyati
Faculty of Engineering, Department of Electrical Engineering,
University of Malaya,
50603 Kuala Lumpur, Malaysia
e-mail: awreza98@yahoo.com

C. Eswaran
Faculty of Information Technology, Multimedia University,
63100 Cyberjaya, Malaysia

Introduction

Eye diseases, such as diabetic retinopathy and glaucoma affect the retina and cause blindness. This condition tends to occur in patients who have had diabetes for five or more years. It is reported that more than half of all newly registered blindness is caused by the retinal diseases and diabetic retinopathy is one of the main contributors [1]. Automatic screening for eye disease has been shown to be very effective in preventing loss of sight. Manual analysis and diagnosis requires a great deal of time and energy to review retinal images which are obtained by fundus camera. Therefore, an automated analysis and diagnosis system will save cost and time significantly considering the large number of retinal images that need to be manually reviewed by the medical professionals each year [2]. In summary, computer-aided analysis can be helpful to assist the screening procedure in detecting diabetic retinopathy and to aid the ophthalmologists when they evaluate or diagnose the fundus images [3]. With this motivation in mind, this paper presents an automatic tracing technique for the boundary detection of bright objects, such as optic disc (OD), exudates, and cotton wool spots in fundus images. The extraction of these objects forms an important step in the diagnosis of eye diseases, such as diabetic retinopathy and glaucoma.

Extraction, detection, and identification of OD, exudates, and cotton wool spots in the fundus images have been one of the main focuses in modern research [3–7]. The detection of the OD in the human retina is a very important task. The OD is the entrance of the vessels and the optic nerve into the retina. It becomes visible in color fundus images as a bright yellowish or white region. Its shape is approximately circular, interrupted by the outgoing vessels. The size of OD differs from patient to patient and its

diameter lies between 40 and 60 pixels in 640×480 color photographs [7]. The diameter delivers a calibration of the measurements [8], and it determines approximately the localization of macula [9], the center of vision, which is of great importance as objects in the macular region affect vision directly. Various methods [7–17], such as high gray level variation, area threshold, Hough transform, back-tracking technique, morphological filtering techniques, watershed transformation, principal component analysis (PCA), and point distribution model have been reported for the detection and extraction of OD. On the other hand, there is extensive research on developing and improving the image processing algorithms for the detection of exudates in retinal images [5–7]. Hard exudates are yellowish intraretinal deposits, which are usually located in the posterior pole of the fundus image. The exudates are made up of serum lipoproteins, considered to leak from the abnormally permeable blood vessels, especially across the walls of leaking microaneurysms. Hard exudates may be observed in several retinal vascular pathologies, but are a main feature of diabetic macular edema [7]. In fact, diabetic macular edema is the main reason of visual impairment in diabetic patients. The most effectual way to diagnose the macular edema is to detect the hard exudates, which are normally associated with macular edema. The exudates are well contrasted relating to the background that surrounds them, and their shape and size vary significantly. The cotton wool spots or soft exudates are infractions in the nerve fiber layers of the retina, which are round or oval in shape, pale yellow-white in color, and are results of capillary occlusions that cause permanent damages to the function of the retina [18]. Hard and soft exudates can be distinguished because of their color and the sharpness of their borders. Various methods [8, 19, 20], such as shade correction, contrast enhancement, sharpening, combination of local and global thresholding, color normalization, fuzzy C-means clustering, and neural networks have been reported for the detection and classification of exudates. However, in this study, the parameters 'number' and 'size' (refer to "Proposed methodology") are taken into account to differentiate and quantify the hard exudates and the cotton wool spots in the fundus images.

In this paper, a new technique for the detection of OD, exudates, and cotton wool spots in ocular fundus images is proposed. The proposed method makes use of: (1) preprocessing algorithms to make the bright object features more distinguishable from the background, (2) markers to modify the gradient image to control oversegmentation, and (3) watershed segmentation to trace the boundary from the marker modified gradient. The proposed method has the following advantages compared to Walter's method [7] and our existing method [5]: (1) there is no need to select different threshold value for different test images those of which are varying with different brightness and contrast conditions (the method proposed in this study only relies on H-minima, which requires a fixed threshold), (2) it automatically segments (does not require manual interaction) all bright lesions in a colour fundus image with the possibility to distinguish between hard exudates and cotton wool spots, (3) the proposed method gives an average sensitivity value of about 95%, which is comparable to [7] and [5], and (4) it will be very useful in the development of computer based automatic screening systems for the early diagnosis of diabetic retinopathy.

The first part of this introductory section is dedicated to the discussion of the ways in which automated image processing technique can contribute to the diagnosis of diabetic retinopathy, and also highlights the properties and state of the art of OD, hard exudates, and cotton wool spots. The organization of the remaining part of this paper is as follows: in "Proposed methodology", the methodology for detecting bright objects from the fundus images is presented. "Results and discussion" presents the test results. Moreover, it includes a comparative performance study with a known method [7] and also with those obtained by human experts. Finally, "Conclusions" concludes the paper along with suggestions for foreseeable future work.
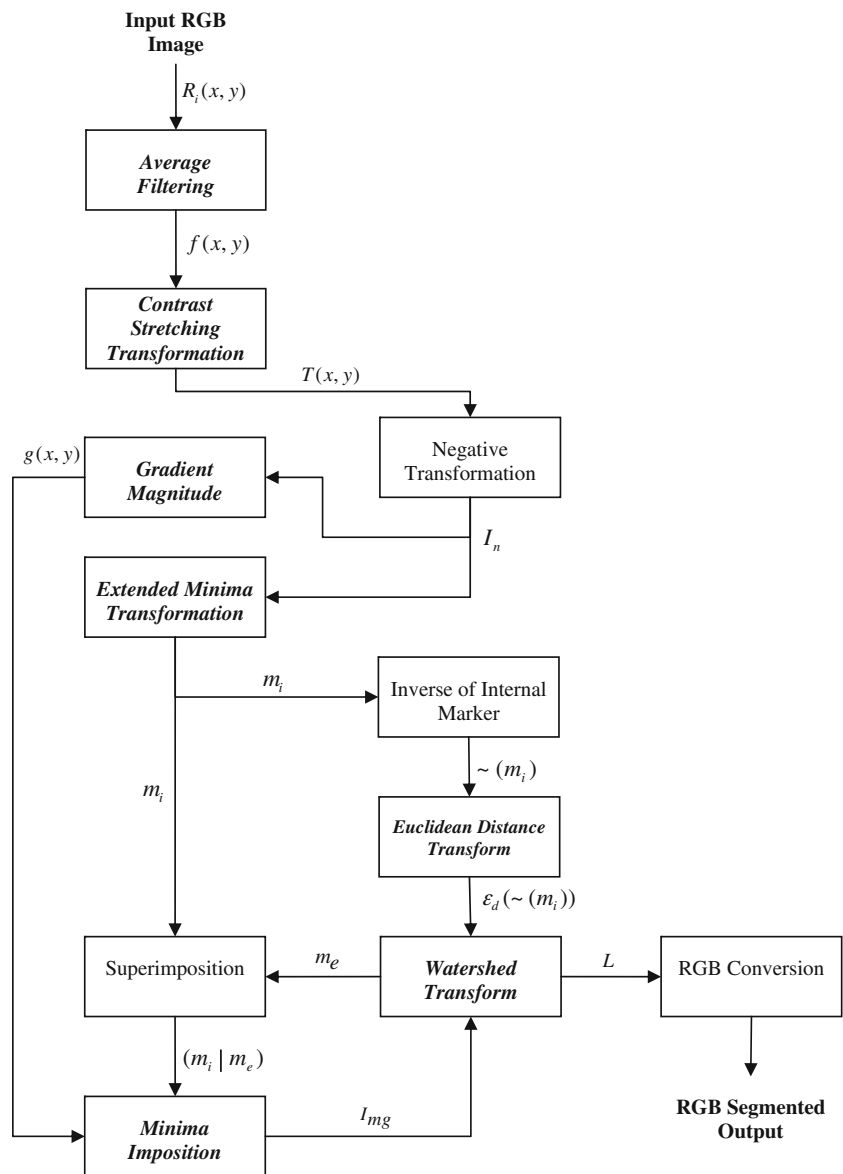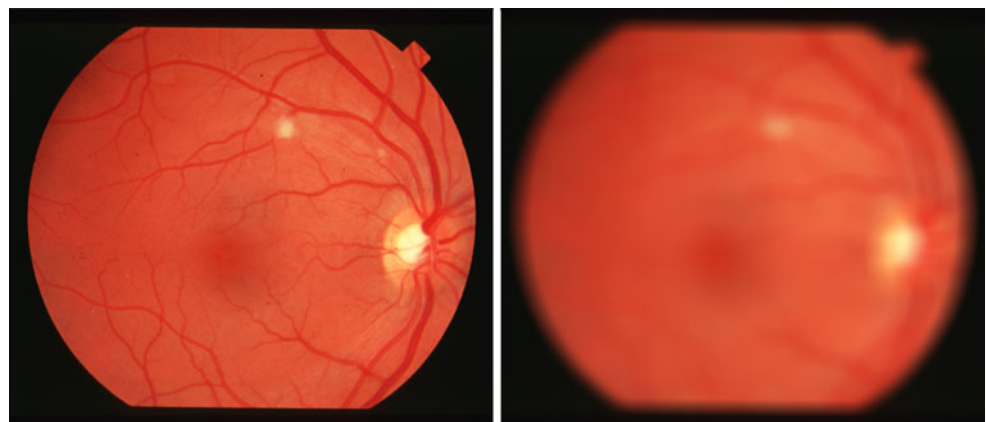
Proposed methodology

Figure 1 shows flow chart of the proposed method with symbol for input and output.

Average filtering

In the original fundus image (Fig. 2a), the intensity variation between the bright objects and the blood vessels is relatively high and the vessels usually have poor local contrast with respect to the background. To isolate the OD and other bright parts is a fundamental problem and hence, preprocessing of the image for subsequent analysis becomes extremely crucial. Therefore, in the first phase, an averaging filter of size 25×35 pixels (the parameter is set by using trial and error procedure on several images) containing equal weights of value "1" is applied to the original image $R_i(x, y)$ (where $i \in 1$–25×35) in order to blend the small objects with low intensity variations into the background, while leaving the objects of interest relatively unchanged. The average filter is implemented using the following Eq. 1 [5, 21].

$$f(x,y) = \frac{1}{M \times N} \sum_{i=1}^{M \times N} R_i(x, y) \tag{1}$$

Fig. 1 Phases of the proposed algorithm

Input RGB Image

$R_i(x, y)$

Average Filtering

$f(x, y)$

Contrast Stretching Transformation

$T(x, y)$

Negative Transformation

I_n

$g(x, y)$ → **Gradient Magnitude**

Extended Minima Transformation

m_i → Inverse of Internal Marker

$\sim (m_i)$

Euclidean Distance Transform

$\varepsilon_d (\sim (m_i))$

m_i

Superimposition ← m_e — **Watershed Transform** — L → RGB Conversion

$(m_i \mid m_e)$

Minima Imposition — I_{mg}

RGB Segmented Output

Fig. 2 a Original image; **b** Average filtered image

(a)   (b)

where $M=25$ and $N=35$. In Eq. 1, average filtering uses a 25×35 mask and then take average of all values within the mask to obtain the effect at each point (x, y) in the original image. The resultant image $f(x, y)$ after applying average filter in Eq. 1 is shown in Fig. 2(b). As shown from Fig. 2 (b), the small objects are blended into the background and the objects of interest are relatively unchanged.

Contrast stretching transformation

As the green channel contains good contrast between the background and the bright retinal components, it is reliable to work on the green channel of the RGB color space in order to localize the OD and exudates [5, 10, 21]. The green component is extracted from the RGB color image as shown in Fig. 3(a). This image is then automatically enhanced by applying the contrast stretching transformation shown in Fig. 3(b) to make the bright object features more distinguishable from the background. In this transformation, only the darker regions have their intensity values enhanced slightly while the brighter regions of the image remain more or less unchanged. The result is an image of higher contrast, which is achieved by using the contrast stretching transform function as shown below [5, 21].

$$T(x,y) = \beta \times [f(x,y)]^n \tag{2}$$

where $f(x, y)$ and $T(x, y)$ represent the input and output (processed) pixel intensity values, respectively, $0 \le n \le 1$, and $\beta = inmax^{1-n}$, where $inmax$ is the desired upper limit intensity value in the output image. The resulting transformed image $T(x, y)$ is shown in Fig. 4(a). In the contrast stretching transformation, the parameter of n equals "1" in Eq. 2. In this case, low intensity values of the darker regions have enhanced their intensity values gradually until

it reaches maximum limit intensity value $inmax$ as indicated in Fig. 3(b).

Gradient magnitude

Figure 4(b) is obtained from Fig. 4(a) by applying a negative transform. The watershed transform can be applied to find catchment basins and watershed ridge lines in the image of Fig. 4(b), which treats the image as a surface where the light pixels (background pixels) have high intensity values and the dark pixels (object pixels) have low intensity values. The image shown in Fig. 4(b) contains several dark blobs. The gradient magnitude is used to preprocess the image prior to using the watershed transform for segmentation. By computing the gradient magnitude of Fig. 4(b) using a linear filter (e.g., Sobel [7, 22]), we obtain Fig. 5(a). It is seen from Fig. 5(a) that the gradient magnitude image $g(x, y)$ has high pixel values along the edges and low pixel values everywhere else. If watershed transform is directly applied on Fig. 5(a), we would get an image as shown in Fig. 5(b), which contains too many watershed ridge lines that do not correspond to the objects in which we are interested. Direct application of the watershed transform to a gradient image usually leads to oversegmentation due to noise and other local irregularities of the gradient [22].

We can see that the image in Fig. 5(b) is severely oversegmented, due to the presence of a large number of regional minima. To control the oversegmentation, an approach based on the concept of markers [7, 22] is made use of. A marker is a connected component belonging to an image. We identify two types of markers, namely, internal markers (associated with objects of interest), and external markers (associated with the background). These markers are then used to modify the gradient image.
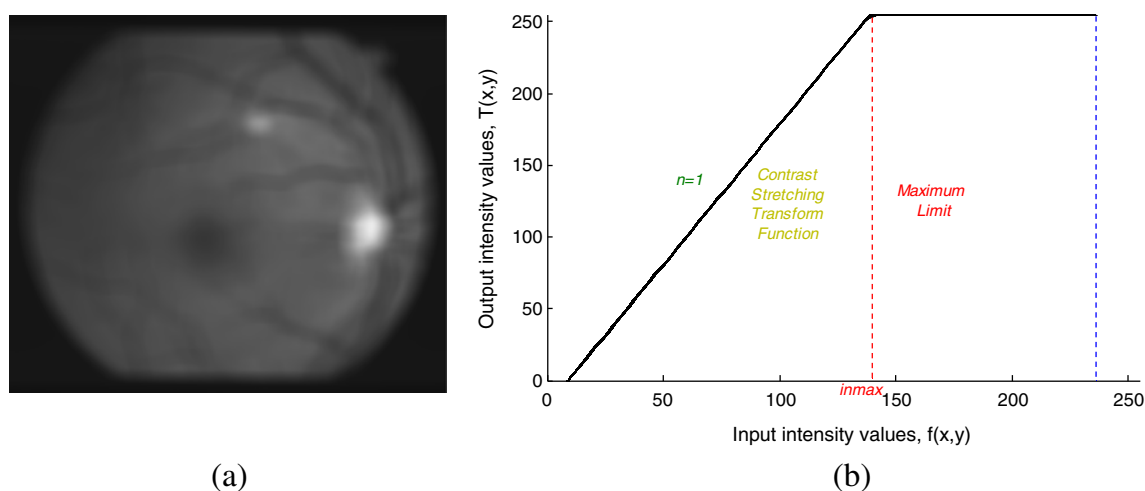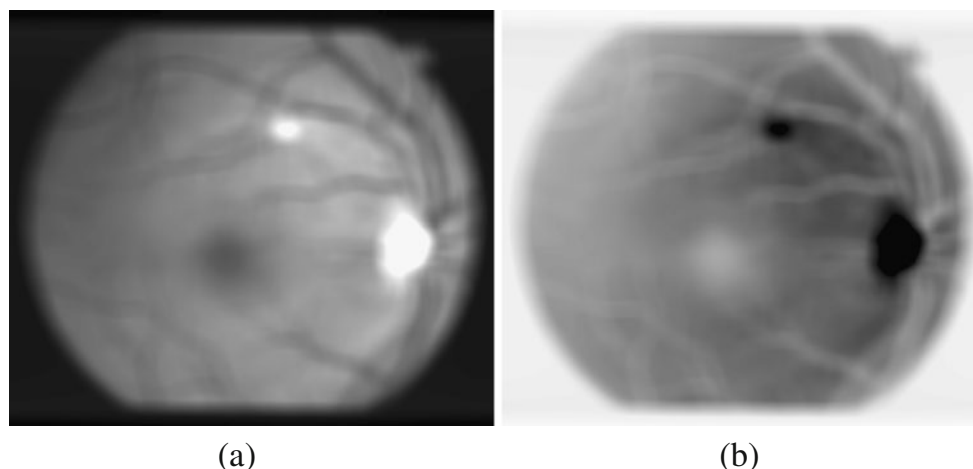

(a)   (b)

Fig. 3 a Green channel; b Contrast stretching transformation

Fig. 4 a Image after contrast adjustment; **b** Negative image of Fig. 4(a)

(a)　　　　　　　　　　　　　　　　　　　(b)

Extended minima transformation

The internal markers m_i shown in Fig. 6(a) are obtained from the negative image of Fig. 4(b) using the extended minima transformation, $f_{imextendedmin}$ [22, 23]. The $f_{imextendedmin}$ computes the extended-minima transform, which is the regional minima of the H-minima transform. In Eq. 3, I_n represents the negative image (Fig. 4b) and H is the height threshold, which requires a fixed parameter (a threshold: $H=2$).

$$m_i = f_{imextendedmin}(I_n, H) \tag{3}$$

The m_i is a binary image whose foreground pixels mark the locations of the deep regional minima. The extended minima transformation determines the groups of brightest pixels belonging to the foreground such that the points in each region form a connected component and all the points in the connected component have the same gray-level value. The internal markers superimpose the extended minima locations as gray blobs on the image of Fig. 4(b) to get the image shown in Fig. 6(b).

Euclidean distance transform

Next, we find external markers [22], or pixels that we are confident belong to the background. The external markers m_e effectively partition the image (Fig. 6a) into regions, with each region contains single internal marker and part of the background. The approach is to mark the background by finding pixels that are exactly midway between the internal markers m_i. The problem is thus reduced to partitioning each of these regions into two: (1) a single object and (2) its background. This can be done by computing the watershed segmentation (WS) of the distance map of the inverse of m_i as shown in Eq. 4.

$$m_e = WS[\varepsilon_d(\sim(m_i))] \tag{4}$$

where ε_d represents the Euclidean distance transform, which is used in conjunction with the watershed transform for segmentation. For each pixel in m_i, the distance transform assigns a number that is the distance between that pixel and the nearest nonzero pixel of m_i. Figure 7(a) shows the

Fig. 5 a Gradient image; **b** Oversegmentation resulting from applying the watershed transform to Fig. 5(a)
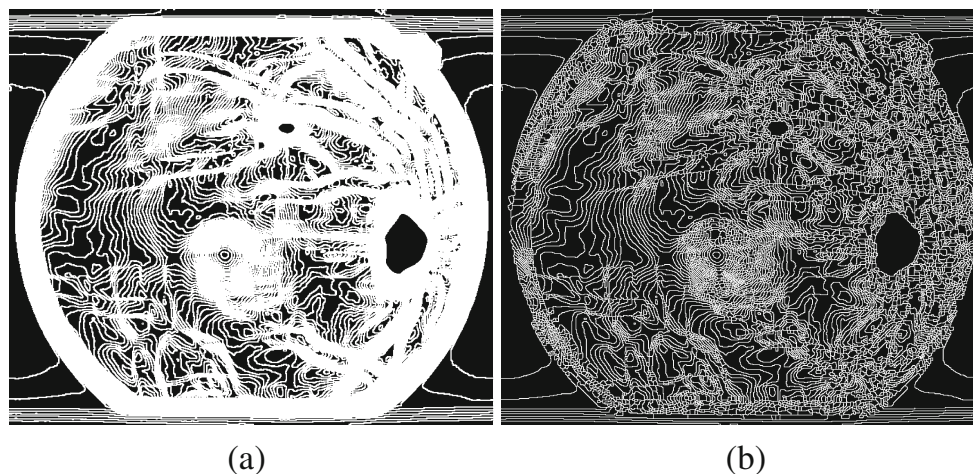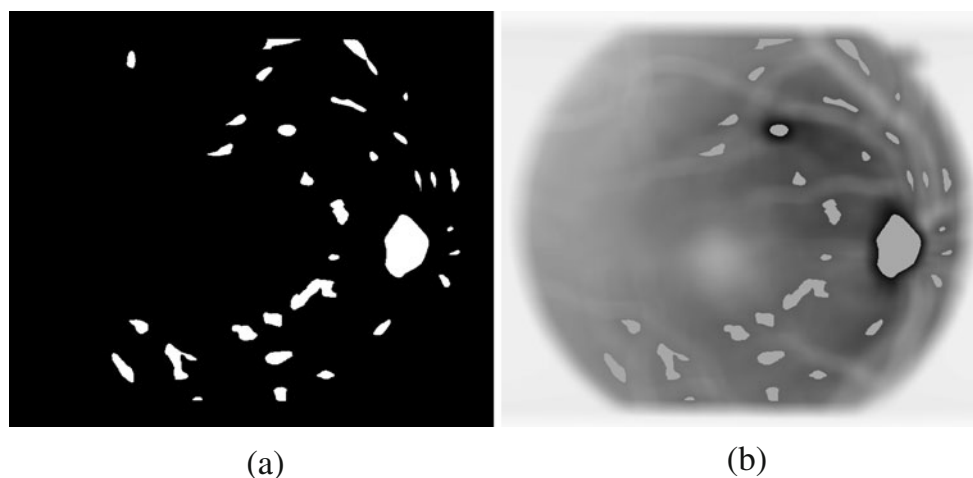

(a)　　　　　　　　　　　　　　　　　　　(b)

(a)   (b)

Fig. 6 a Internal markers; b Superimposition of the internal markers on the image of Fig. 4(b)

resulting watershed ridge lines as external markers in the binary image.

Minima imposition

Given both internal markers and external markers, the gradient image $g(x, y)$ of Fig. 5(a) is modified using a procedure called minima imposition, $f_{imposemin}$ [22]. This technique modifies the image so that regional minima occur only in marked location. Other pixels values are pushed up as necessary to remove all other regional minima. We modify the gradient image by imposing regional minima at the locations of both the internal and the external markers as shown in Eq. 5.

$$I_{mg} = f_{imposemin}(g(x,y), (m_i|m_e)) \qquad (5)$$

where $f_{imposemin}$ modifies the gradient image $g(x, y)$ using morphological reconstruction so that it only has regional minima wherever superimposition (denoted by logical "or")

of m_i and m_e i.e., $(m_i|m_e)$ is nonzero. The modified gradient image I_{mg} is shown in Fig. 7(b).

Watershed transform

We finally compute the watershed transform of the marker modified gradient image I_{mg} of Fig. 7(b) as follows.

$$L = WS(I_{mg}) \qquad (6)$$

The watershed transformed image L, then superimposes the watershed ridge lines on the image of Fig. 4(b) to get the image shown in Fig. 8(a). The image of Fig. 8(a) is converted into an RGB color image as shown in Fig. 8(b), for the purpose of visualizing the labeled regions (the objects of interest).

To differentiate OD, exudates, and cotton wool spots from other bright areas detected in the background, the technique (a procedure [24] to convert label matrix of Fig. 8 (a) that is returned by watershed, into an RGB color image) determines the color to assign to each object based on the

(a)   (b)

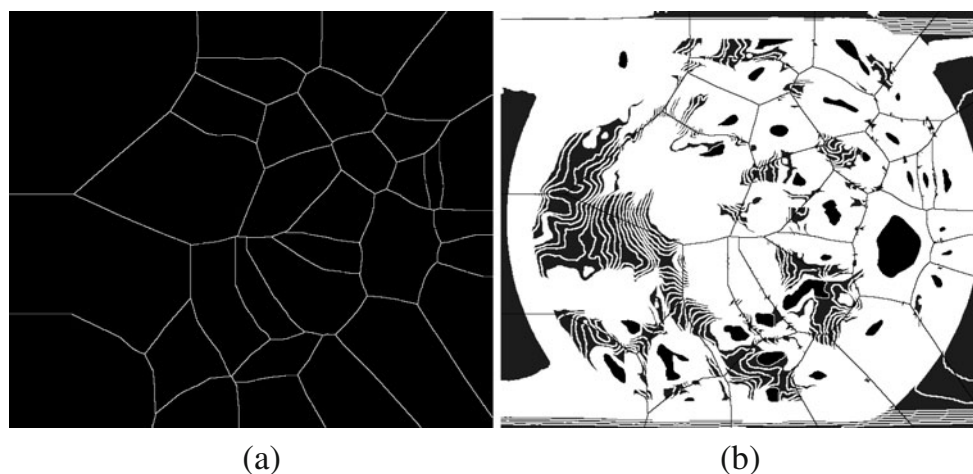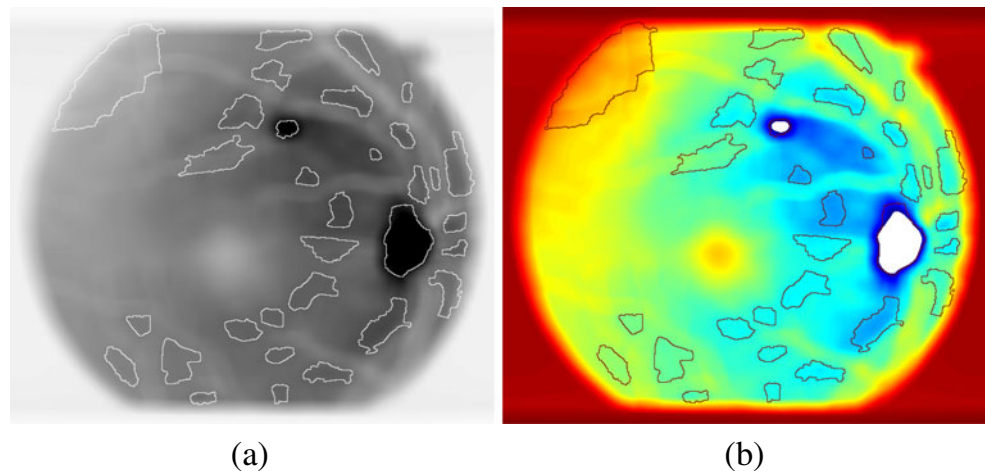Fig. 7 a External markers; b Modified gradient magnitude

Fig. 8 **a** Watershed segmentation result; **b** Segmentation result in RGB color space

(a)   (b)

number of objects in the label matrix and range of colors in the colormap. The procedure picks colors from the entire range. The objects with similar characteristics are filled up with the same color. Therefore, the objects filled with white color within the marked region represent the brightest regions of interest, such as OD, exudates, and cotton wool spots. The additional markers in Fig. 8(b) represent other bright pixels (as the external marker uses a larger area than the diameters of the OD and exudates) of the retinal image that belong to the background.

In our study, two features are identified to distinguish the hard exudates and the cotton wool spots. These two features are '*size*' and '*number*' (refer to Table 1). The representations of the feature values are given as follows:

size: value indicates the number of pixels covered.
number: value indicates the number of bright lesions.

In this study, hard exudates and cotton wool spots are distinguished because of their size and the number of occurrence in the fundus image. Obviously, the features '*size*' and '*number*' are sufficient to quantify the hard exudates and the cotton wool spots. In order to define the hard exudates and the cotton wool spots in this case study (refer to Table 1), the feature, such as number of hard exudates or size of hard exudates (if size exceeds the *value* of 150 as the parameter is set by using trial and error procedure on several images) is present, and in addition to

this, number of cotton wool spots or size of cotton wool spots (if size is below the *value*) is present.

Results and discussion

The method described in the previous section has been tested on images of publicly available DRIVE and STARE databases. The software tools selected are from the MATLAB Image Processing Toolbox (IPT) [24]. Figure 9 shows some samples of the segmented images obtained by using the proposed method.

The performance of the proposed algorithm is evaluated on the basis of three measures: (1) true positive fraction (TPF), (2) true negative fraction (TNF), and (3) predictive value (PV). TPF represents the fraction of pixels correctly classified as OD, exudate, and cotton wool spot pixels. This measure is also known as sensitivity [5, 21]. TNF (also known as specificity) represents the fraction of pixels erroneously classified as OD, exudate, and cotton wool spot pixels [5, 21]. PV is the probability that a pixel which has been classified as OD, exudate, and cotton wool spot is really an OD, exudate, and cotton wool spot [5, 21]. The three measures are calculated using the following equations [5, 7, 21].

$$TPF = \frac{TP}{TP + FN} \tag{7}$$

$$TNF = \frac{TN}{TN + FP} \tag{8}$$

$$PV = \frac{TP}{TP + FP} \tag{9}$$

where *TP*, *FN*, *TN*, and *FP* represent true positive, false negative, true negative, and false positive values. The TPF,

Table 1 Definition of hard exudates and cotton wool spots

Lesion	Definition
HE	Small *size* (> *value*) & *number* ≥1 (in most cases, number of occurrence of HE in fundus images is higher than CWS)
CWS	Smaller *size* (< *value*) & *number* ≥1

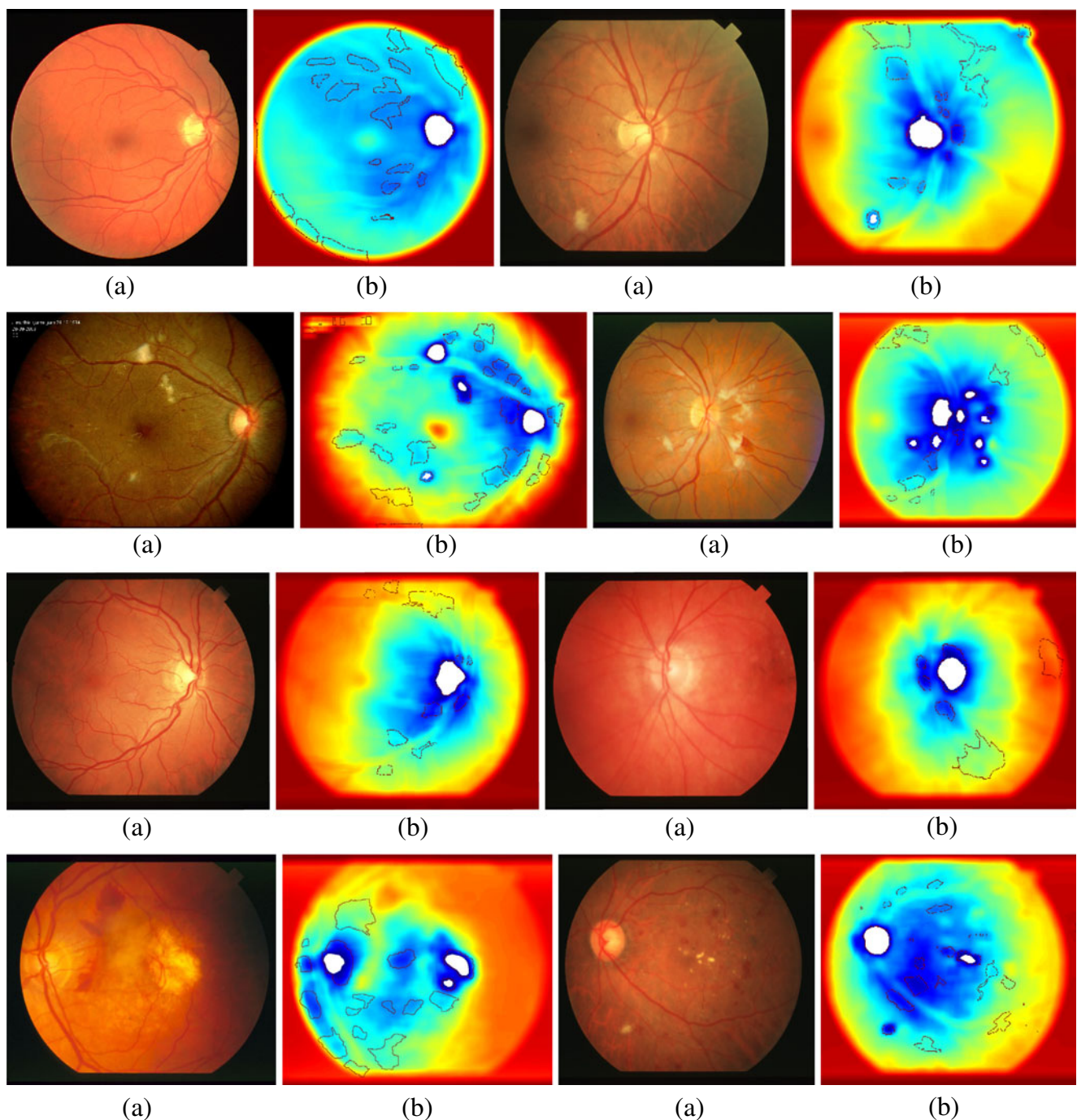*HE* hard exudates; *CWS* cotton wool spots

Fig. 9 **a** Original image; **b** Segmented image

TNF, and PV values are determined using human graded images as reference images. Figure 10 shows the sensitivity, specificity, and the predictive values obtained using the proposed method on different images of DRIVE and STARE databases.

Table 2 shows the sample images in terms of different categories of bright lesions along with their feature characteristics. A total of 20 fundus images related to

diabetic retinopathy are selected from DRIVE and STARE databases for comparison. Table 3 compares the detection results obtained by our proposed system with those obtained or judged by the human experts (ophthalmologist and surgeon from the medical center). It is found that the results obtained by the proposed method are comparable to those obtained by others. The results analysis further reveals that, 16 out of 20 fundus images are correctly

Fig. 10 The TPF, TNF, and PV values on different images of DRIVE and STARE databases
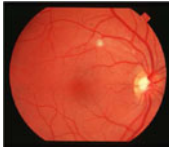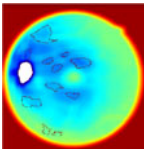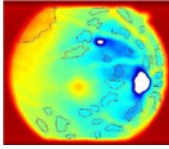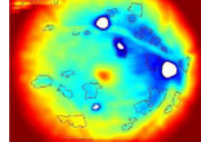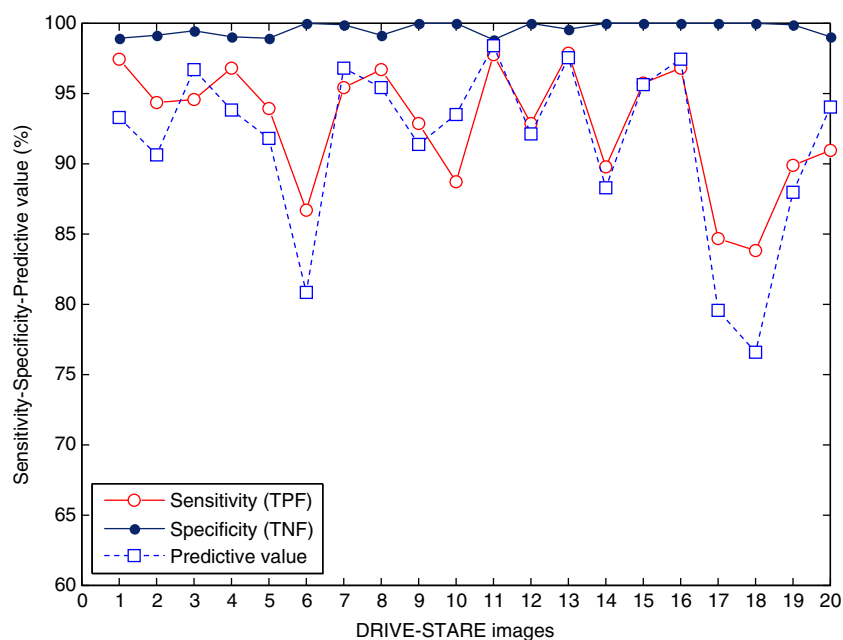

detected by the proposed screening system. The correct sorting rate (which is defined as the percentage of times the algorithm finds the correct features over a number of sample images) for this simulation yields 80%, which indicates that only four images are wrongly sorted (highlighted by yellow color in Table 3). The misdetections are due to poor image quality (as OD is not bright in some cases) or uncalibrated image processing.

The results obtained using the proposed method is also compared with those obtained by using Walter's method [7]. To perform fair comparison between the proposed method and Walter's method, we have implemented Walter's method on the same test images of DRIVE and STARE databases to obtain Fig. 11. Thus, Fig. 11 compares the sensitivity values and the PV values obtained for test images using both the methods. Table 4 shows the average values for sensitivity, specificity, and the PV obtained using the proposed method and Walter's method [7]. From Fig. 11 and Table 4, we note that the proposed method gives better sensitivity or TPF values compared to Walter's method [7] based on the test images from DRIVE and STARE databases. For both the methods, high specificity

Table 2 Feature characteristics for the bright lesions

Feature Name	OD	OD, HE	OD, HE, CWS
Size	-	small (HE)	smaller (CWS)
Number	-	HE=1	HE=2, CWS=1
Sample Image			

Note: OD = Optic Disc; HE = Hard Exudates; CWS = Cotton Wool Spots

Table 3 Performance comparison with reference images detected by human experts

Image ID	Detected Features (Human Experts)	Detected Features (Proposed Method)
im100	OD, HE	OD, HE
im0008	OD, HE	OD, HE
im110	OD, HE, CWS	OD, HE, CWS
im0149	OD, HE	HE
im0102	OD, HE	OD, HE
im0022	OD	OD
im0023	OD	OD
im0048	OD, HE, CWS	OD, HE, CWS
02_test	OD	OD
11_test	OD	OD
im0016	OD, HE	OD, HE
im0148	OD, HE	HE
im0013	OD, HE, CWS	OD, HE, CWS
13_test	OD	OD
im0143	OD, HE	HE
im113	OD, HE	OD, HE
im111	OD, HE	OD, HE
im112	OD, HE	OD, HE
im103	OD, HE	HE
im104	OD, HE	OD, HE

OD optic disc; *HE* hard exudates; *CWS* cotton wool spots

Fig. 11 Performance comparison of both the methods with respect to TPF value and PV
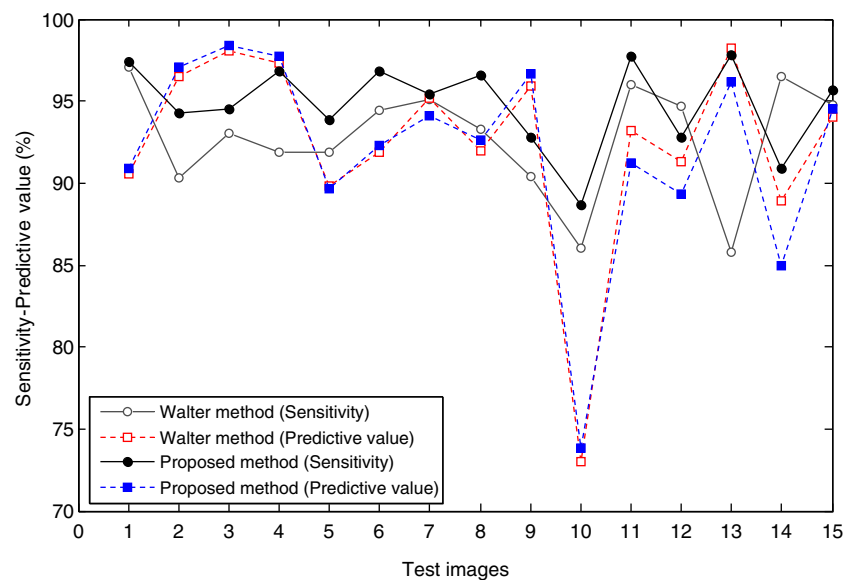
Table 4 Performance of segmentation techniques on DRIVE and STARE databases

Method	TPF value (sensitivity)	TNF value (specificity)	PV (predictive value)
Walter [7]	92.74%	100%	92.39%
Proposed method	94.90%	100%	92.01%

(almost 100%) values have been obtained. With respect to PV, the values obtained by both the methods do not differ significantly.

Conclusions

This paper describes a new method for automatic detection of OD and other bright lesions, such as hard exudates and cotton wool spots in colour fundus images, which is a very important subject in computer assisted diagnosis of retinal diseases. The method consists in three steps: preprocessing, marker construction, and the watershed algorithm. Basically, the described method consists in applying a classical marker controlled watershed transformation after pre-filtering step. The originality or novelty of the paper mainly relies on the selection of the markers, which successfully match the OD and exudates. The results are then compared with the results obtained by a previously published method. The experimental results on DRIVE and STARE databases show that the proposed method yields better sensitivity values compared to Walter's method. In comparison with the detection results obtained by the human experts, the proposed method yields correct sorting rate of 80%.

From a medical point of view, it segments all bright patterns in a colour fundus image with the possibility to distinguish between the lesions (e.g., between hard exudates and cotton wool spots); which is actually an advantage. Hence, the method can be applied for computer assisted diagnosis of retinal diseases. In the future, for instance, it is of interest to distinguish between normal and pathological retinas with the proposed method.

References

1. Reza, A. W., Eswaran, C., and Hati, S., Diabetic retinopathy: A quadtree based blood vessel detection algorithm using RGB components in fundus images. *J. Med. Syst.* 32(2):147–155, 2008.
2. Teng, T., Lefley, M., and Claremont, D., Progress towards automated diabetic ocular screening: A review of image analysis and intelligent systems for diabetic retinopathy. *Med. Biol. Eng. Comput.* 40:2–13, 2002.
3. Yen, G. G., and Leong, W.-F., A sorting system for hierarchical grading of diabetic fundus images: A preliminary study. *IEEE Trans Inf Technol Biomed* 12(1):118–130, 2008.
4. Usher, D., Dumskyj, M., Himaga, M., Williamson, T. H., Nussey, S., and Boyce, J., Automated detection of diabetic retinopathy in digital retinal images: A tool for diabetic retinopathy screening. *Diabet. Med.* 21:84–90, 2003.
5. Reza, A. W., Eswaran, C., and Hati, S., Automatic tracing of optic disc and exudates from color fundus images using fixed and variable thresholds. *J. Med. Syst.* 33(1):73–80, 2009.
6. Eswaran, C., Reza, A. W., and Hati, S., Extraction of the contours of optic disc and exudates based on marker-controlled watershed segmentation. *Proceedings of the International Conference on Computer Science and Information Technology*, Singapore, pp. 719–723, 2008.
7. Walter, T., Klein, J.-C., Massin, P., and Erginay, A., A contribution of image processing to the diagnosis of diabetic retinopathy—Detection of exudates in color fundus images of the human retina. *IEEE Trans. Med. Imag.* 21(10):1236–1243, 2002.
8. Ward, N. P., Tomlinson, S., and Taylor, C. J., Image analysis of fundus photographs—The detection and measurement of exudates associated with diabetic retinopathy. *Opthalmol.* 96:80–86, 1989.
9. Akita, K., and Kuga, H., A computer method of understanding ocular fundus images. *Pattern Recogn.* 15(6):431–443, 1982.
10. Sinthanayothin, C., Boyce, J. F., Cook, H. L., and Williamson, T. H., Automated localization of the optic disc, fovea and retinal blood vessels from digital color fundus images. *Br. J. Opthalmol.* 83:231–238, 1999.
11. Tamura, S., and Okamoto, Y., Zero-crossing interval correction in tracing eye-fundus blood vessels. *Pattern Recogn.* 21(3):227–233, 1988.
12. Pinz, A., Prantl, M., and Datlinger, P., Mapping the human retina. *IEEE Trans. Med. Imag.* 1:210–215, 1998.
13. Mendels, F., Heneghan, C., and Thiran, J.-P., Identification of the optic disc boundary in retinal images using active contours. *Proceedings of Irish Machine Vision image Processing (IMVIP)*, Maynooth, Ireland, pp. 103–115, 1999.
14. Walter, T., and Klein, J. C., Segmentation of color fundus images of the human retina: Detection of the optic disc and the vascular tree using morphological techniques. *Proceedings of the second International Symposium: Medical Data Analysis*, Madrid, Spain, pp. 282–287, 2001.
15. Li, H., and Chutatape, O., Automatic detection and boundary estimation of the optic disk in retinal images using a model-based approach. *J. Electron. Imag.* 12(1):97–105, 2003.
16. Li, H., and Chutatape, O., Automated feature extraction in color retinal images by a model based approach. *IEEE Trans. Biomed. Eng.* 51(2):246–254, 2004.
17. Niemeijer, M., Abramoff, M. D., and van Ginneken, B., Segmentation of the optic disc, macula and vascular arch in fundus photographs. *IEEE Trans. Med. Imag.* 26(1):116–127, 2007.
18. Vallabha, D., Dorairaj, R., Namuduri, K., and Thompson, H., Automated detection and classification of vascular abnormalities in diabetic retinopathy. *Proceedings of Thirty-Eighth Asilomar Conference on Signals, Systems and Computers*, vol. 2, pp. 1625–1629, 2004.
19. Phillips, R., Forrester, J., and Sharp, P., Automated detection and quanification of retinal exudates. *Graefe's Arch. Clin. Exp. Opthalmol.* 231:90–94, 1993.
20. Osareh, A., Mirmehdi, M., Thomas, B., and Markham, R., Automatic recognition of exudative maculopathy using fuzzy c-means clustering and neural networks. *Proceedings of Medical Image Understanding Analysis*, UK, pp. 49–52, 2001.
21. Reza, A. W., and Eswaran, C., A decision support system for automatic screening of non-proliferative diabetic retinopathy. *J. Med. Syst. Springer*, 2009. doi:10.1007/s10916-009-9337-y.
22. Gonzalez, R. C., Woods, R. E., and Eddins, S. L., *Digital image processing using MATLAB*. Prentice Hall, Upper Saddle River, 2004.
23. Soille, P., *Morphological image analysis: principles and applications*, 2nd edition. Springer-Verlag, New York, 2002.
24. Image Processing Toolbox, User's Guide, Version 4, The Math Works, Inc., Natick, MA, 2003.